Check for updates

Turbofan Engine Sizing and Tradeoff Analysis via Signomial Programming

Martin A. York,* Warren W. Hoburg,† and Mark Drela‡
Massachusetts Institute of Technology, Cambridge, Massachusetts 02139

DOI: 10.2514/1.C034463

This paper presents a full one-dimensional core and fan flowpath turbofan optimization model, based on first principles, and meant to be used during aircraft conceptual design optimization. The model is formulated as a signomial program, which is a type of optimization problem that can be solved locally using sequential convex optimization. Signomial programs can be solved reliably and efficiently and are straightforward to integrate with other optimization models in an all-at-once manner. To demonstrate this, the turbofan model is integrated with a simple commercial aircraft sizing model. The turbofan model is validated against the Transport Aircraft System Optimization turbofan model as well as two Georgia Institute of Technology Numerical Propulsion System Simulation turbofan models. Four integrated engine/aircraft parametric studies are performed, including a multimission optimization with over 2400 variables that solves in under 4 s.

Downloaded by MASSACHUSETTS INST OF TECHNOLOGY on November 24, 2017 | http://arc.aiaa.org | DOI: 10.2514/1.C034463

Nomenclature

A	=	flow area
a	=	speed of sound
C_D	=	aircraft drag coefficient
C_L	=	aircraft lift coefficient
C_p	=	working fluid constant pressure specific heat
c_k	=	constant in a monomial, posynomial, or signomial
D	=	drag force
F	=	total engine thrust
F_{sp}	=	overall specific thrust
f_c	=	cooling flow bypass ratio ($\dot{m}_{cool}/\dot{m}_{core}$)
F_6	=	core engine thrust
F_8	=	fan engine thrust
f_f	=	fuel/air ratio
$\bar{f}_o$	=	1 minus the percent of core mass flow bled for pressurization, electrical generation, etc.
G_f	=	fan gearing ratio
h, h_t	=	static and stagnation enthalpy
h_f	=	fuel heat of combustion
M	=	Mach number
$\dot{m}$	=	mass flow
$\bar{m}$	=	corrected mass flow
$m(u)$	=	monomial function of u
m_{engine}	=	engine mass
N_f	=	normalized fan spool speed
N_1	=	normalized low-pressure compressor spool speed
N_2	=	normalized high-pressure compressor spool speed
P, P_t	=	static and stagnation pressure
$p(u)$	=	posynomial function of u
R	=	specific gas constant
r_{uc}	=	cooling flow velocity ratio
$s(u)$	=	signomial function of u
T, T_t	=	static and stagnation temperature
TSFC	=	thrust-specific fuel consumption
$\boldsymbol{u}$	=	vector of all decision variables
u	=	flow velocity
V	=	aircraft velocity
W_{engine}	=	engine weight
Z	=	total/static temperature ratio
α	=	engine bypass ratio
γ	=	ratio of working fluid specific heats
η	=	efficiency
$\pi_{(\cdot)}$	=	pressure ratio across component $(\cdot)$
ρ	=	air density

Subscripts

b	=	combustor quantity
cool	=	cooling flow quantity
core	=	core stream quantity
D	=	nominal design point quantity
d	=	diffuser quantity
f	=	fan quantity
fan	=	fan stream quantity
fn	=	fan nozzle quantity
HP	=	high-pressure shaft quantity
HPC	=	high-pressure compressor quantity
i	=	quantity at engine station i
LP	=	low-pressure shaft quantity
LPC	=	low-pressure compressor quantity
SL	=	sea-level quantity
t	=	stagnation quantity
total	=	fan and core stream quantity
$+1$	=	plus one

Received 8 March 2017; revision received 23 August 2017; accepted for publication 15 September 2017; published online 9 November 2017. Copyright © 2017 by Martin York, Warren Horburg, and Mark Drela. Published by the American Institute of Aeronautics and Astronautics, Inc., with permission. All requests for copying and permission to reprint should be submitted to CCC at www.copyright.com; employ the ISSN 0021-8669 (print) or 1533-3868 (online) to initiate your request. See also AIAA Rights and Permissions www.aiaa.org/randp.

*Graduate Student, Department of Aeronautics and Astronautics.
†Assistant Professor, Department of Aeronautics and Astronautics; currently Astronaut Candidate, NASA, Houston, Texas 77058. Member AIAA.
‡Terry J. Kohler Professor, Department of Aeronautics and Astronautics. Fellow AIAA.

I. Introduction

A KEY goal of conceptual aircraft design is to quantify basic tradeoffs between competing mission requirements and between the various aircraft subsystems. For an exhaustive study, multiple design parameter sweeps must be performed, ideally with an optimum conceptual aircraft produced for each point examined. Because typical aircraft design-parameter spaces are quite large, such trade studies demand a reliable and efficient system-level optimization method. As noted by Martins and Lambe [1], there exists a need for new multidisciplinary design optimization (MDO) tools that exhibit fast convergence for medium- and large-scale problems. In pursuit of this goal, Hoburg and Abbeel [2] and Kirschen et al. [3] have proposed formulating aircraft conceptual design models as geometric programs (GPs) or signomial programs (SPs). Geometric and signomial programs enable optimization problems with thousands of design variables to be reliably solved on laptop computers in a matter of seconds.

Such speed and reliability are possible because these formulations can be solved via convex optimization (in the case of GP) or via

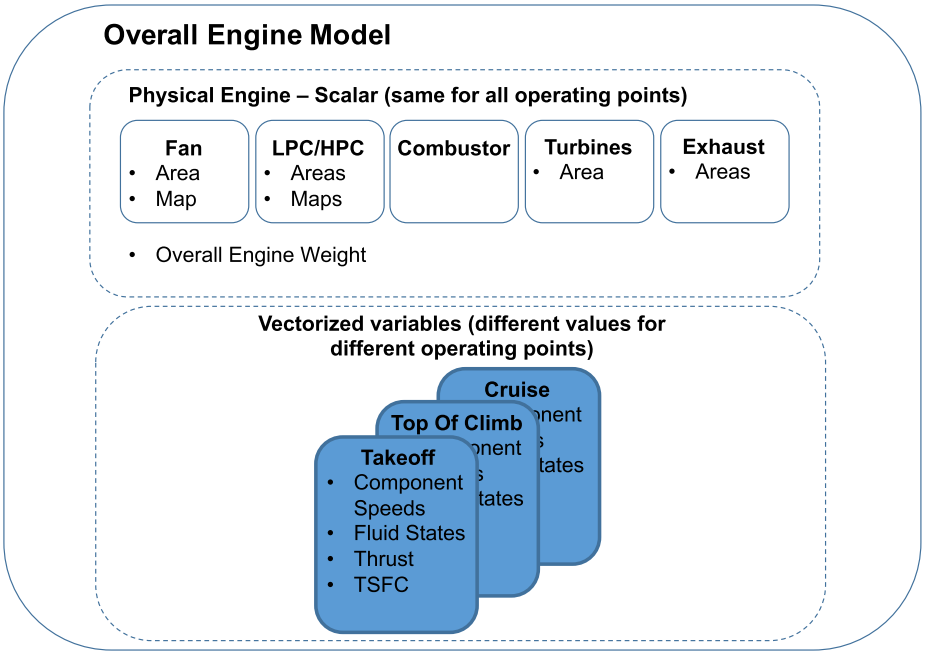

Fig. 1 Engine model architecture.

Downloaded by MASSACHUSETTS INST OF TECHNOLOGY on November 24, 2017 | http://arc.aiaa.org | DOI: 10.2514/1.C034463

sequential convex optimization (in the case of SP). One limitation of GP methods is that all physical model equations must be posed as either posynomial inequality constraints or monomial equality constraints, which at first seems far too restrictive. One objective of this paper is to show that this is not necessarily the case and that even quite complex physical models can be recast into the necessary forms. This is accomplished in two ways. First, many, but not all, expressions that arise in turbofan design are directly compatible with GP or can be closely approximated by posynomial constraints. Second, relationships that are not directly GP-compatible are often SP-compatible. SP is a nonconvex extension of GP that can be solved locally as a sequence of GPs. Although SPs sacrifice guarantees of global optimality, they can be solved far more reliably than general nonlinear programs.

The specific example considered is the turbofan model in the Transport Aircraft System Optimization (TASOPT) [4] conceptual design tool, which uses traditional optimization techniques. This model is a full 1-D core and fan flowpath simulation based on first principles, which here will be recast into an SP-compatible form. This enables the construction of SP-compatible aircraft conceptual design models that address the complex design tradeoffs between engine and airframe parameters by treating the parameters as design variables. Such methods can produce much more realistic and higher-fidelity conceptual designs as starting points for subsequent preliminary and detailed design, with more reliability and much less time than would be required by the alternative MDO methods that combine traditional engine and airframe modules.

The SP-compatible engine model developed here is compared against TASOPT and two Georgia Institute of Technology Numerical Propulsion System Simulation (NPSS) [5] models to demonstrate that it produces the correct results. To demonstrate its effectiveness for SP aircraft optimization, the model is integrated into a simple commercial transport aircraft sizing optimization problem. Example aircraft parametric studies are presented, including a 2480-variable multimission optimization problem that solves in 3.71 s.

II. Optimization Formulation

A. Model Architecture

The presented engine model is formulated as a single multipoint optimization problem with no engine on/off design point distinctions. All constraints are applied at every point in the flight, and the model selects the engine that most optimally meets all constraints. This, coupled with the fact that SPs are solved all at once (i.e., there is no order of operations), greatly simplifies integrating the engine into a full aircraft system model. Figure 1 illustrates the engine model's overall architecture. No initial guesses are supplied to the presented model.

B. Solution Method

The models in this paper consist of sets of constraints that are compatible with SP. All SPs presented in this paper were solved on a laptop computer using a combination of GPkit [6] and MOSEK [7]. GPkit, developed at the Massachusetts Institute of Technology, is a python package that enables the fast and intuitive formulation of geometric and signomial programs. GPkit has a built in heuristic for solving SPs as a series of GP approximations. GPkit binds with open-source and commercial interior point solvers to solve individual GPs.

C. Geometric Programming

Introduced in 1967 by Duffin et al. [8], a geometric program (GP) is a type of constrained optimization problem that becomes convex after a logarithmic change of variables. Modern interior point methods allow a typical sparse GP with tens of thousands of decision variables and tens of thousands of constraints to be solved in minutes on a desktop computer [9]. These solvers do not require an initial guess and guarantee convergence to a global optimum, assuming that a feasible solution exists. If a feasible solution does not exist, the solver will return a certificate of infeasibility. These impressive properties are possible because a GP's objective and constraints consist of only monomial and posynomial functions, which can be transformed into convex functions in log space.

A monomial is a function of the form

$$m(\boldsymbol{u}) = c\prod_{j=1}^{n} u_j^{a_j} \tag{1}$$

where $a_j \in \mathbb{R}$, $c \in \mathbb{R}_{++}$, and $u_j \in \mathbb{R}_{++}$. An example of a monomial is the common expression for lift, $(1/2)\rho V^2 C_L S$. In this case, $\boldsymbol{u} = (\rho, V, C_L, S)$, $c = 1/2$, and $a = (1, 2, 1, 1)$.

A posynomial is a function of the form

$$p(\boldsymbol{u}) = \sum_{k=1}^{K} c_k \prod_{j=1}^{n} u_j^{a_{jk}} \tag{2}$$

where $a_{jk} \in \mathbb{R}$, $c_k \in \mathbb{R}_{++}$, and $u_j \in \mathbb{R}_{++}$. A posynomial is a sum of monomials. Therefore, all monomials are also one-term posynomials.

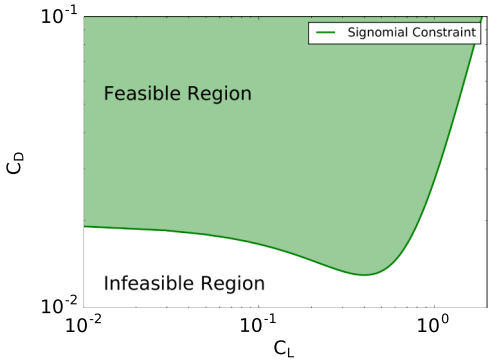

a) Non-convex signomial inequaltiy drag constraint

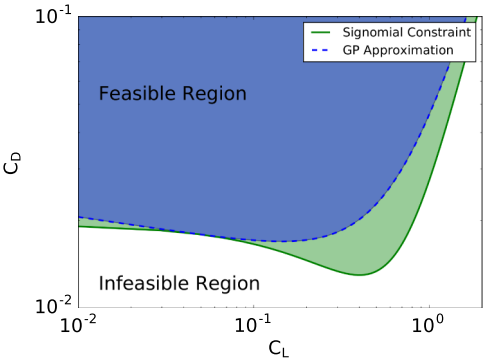

b) Convex approximation about $C_L = 0.05$

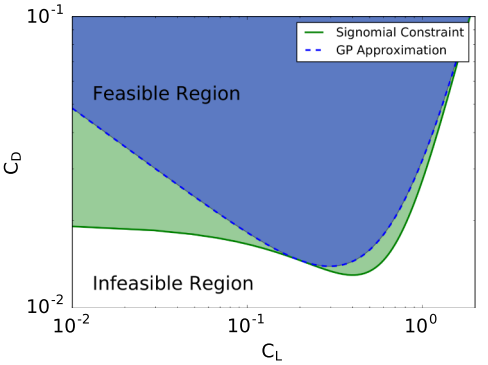

c) Convex approximation about $C_L = 0.20$

Fig. 2 The nonconvex signomial inequality drag constraint $C_D \geq f(C_L)$ and GP approximations about two different points.

A GP minimizes a posynomial objective function subject to monomial equality and posynomial inequality constraints. A GP written in standard form is

$$\begin{aligned} &\text{minimize} && p_0(\boldsymbol{u}) \\ &\text{subject to} && p_i(\boldsymbol{u}) \leq 1, \quad i = 1, \ldots, n_p, \\ &&& m_i(\boldsymbol{u}) = 1, \quad i = 1, \ldots, n_m \end{aligned} \tag{3}$$

where p_i are posynomial functions, m_i are monomial functions, and $\boldsymbol{u} \in \mathbb{R}^n_{++}$ are the decision variables. Once a problem has been formulated in the standard form [Eq. (3)], it can be solved efficiently.

D. Signomial Programming

It is not always possible to formulate a design problem as a GP. This motivates the introduction of signomials. Signomials have the same form as posynomials:

$$s(\boldsymbol{u}) = \sum_{k=1}^{K} c_k \prod_{j=1}^{n} u_j^{a_{jk}} \tag{4}$$

but the coefficients $c_k \in \mathbb{R}$ can now be any (including nonpositive) real numbers.

A signomial program (SP) is a generalization of GP where the inequality constraints can be composed of signomial constraints of the form $s(u) \leq 0$. The log transform of an SP is not a convex optimization problem, but it is a difference of convex optimization problem that can be written in log space as

$$\begin{aligned} &\text{minimize } f_0(\boldsymbol{x}) \\ &\text{subject to } f_i(\boldsymbol{x}) - g_i(\boldsymbol{x}) \leq 0, \quad i = 1, \ldots, m \end{aligned} \tag{5}$$

where f_i and g_i are convex.

There are multiple algorithms that reliably solve signomial programs to local optima [10,11]. This is done by solving a sequence of GPs, where each GP is a local approximation to the SP, until convergence occurs. The introduction of even a single signomial constraint to any GP turns the GP into a SP, thus losing the guarantee of solution convergence to a global optimum. A favorable property of SP inequalities is that the feasible set of the convex approximation is always a subset of the original SP's feasible set, as depicted in Fig. 2. This removes the need for trust regions and makes solving SPs substantially more reliable than solving general nonlinear programs.

The previously presented difference of convex technique works only for signomial inequality, posynomial inequality, and monomial equality or inequality constraints. Signomial equality constraints can be approximated by monomials, as shown in Fig. 3. Signomial equalities are the least desirable type of constraint because the feasible set of their GP approximation in log space is not a subset of the original feasible set. This work contains five signomial equality constraints. For additional

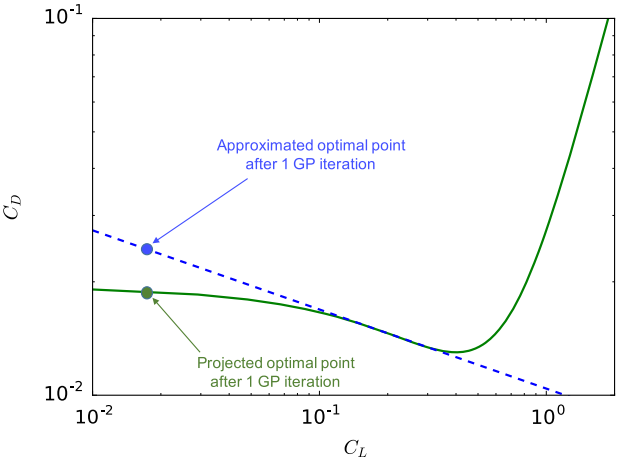

Fig. 3 Signomial equality constraint $C_D = f(C_L)$ and its approximation.

Downloaded by MASSACHUSETTS INST OF TECHNOLOGY on November 24, 2017 | http://arc.aiaa.org | DOI: 10.2514/1.C034463

Downloaded by MASSACHUSETTS INST OF TECHNOLOGY on November 24, 2017 | http://arc.aiaa.org | DOI: 10.2514/1.C034463

details on how signomial equalities are approximated, see Opgenoord et al. [12]. For intuition on when signomial equality constraints are required, see Appendix D.

III. Terminology

Before proceeding, it is useful to introduce some of the vocabulary used to describe this work.

A. Models

A model is a set of GP and/or SP compatible constraints. The input to a model is the value of any fixed variables or constants appearing the model. Two models that share variables may be linked by concatenating their constraints.

B. Geometric and Signomial Programming Compatibility

A constraint is GP-compatible if it can be written as either a monomial equality [Eq. (1)] or a posynomial inequality [Eq. (2)]. A constraint is SP-compatible if it can be written as a signomial inequality [Eq. (4)] or equality.

C. Static and Performance Models

The presented model is a multipoint optimization problem. To formulate the multipoint problem, two models are created for each engine component: a static and a performance model. The static model contains all variables and constraints that do not change between operating points, such as engine weight and nozzle areas. Performance models contain all constraints and variables that do change between operating points. For example, all constraints involving fluid states are contained in performance models. To simulate multiple engine operating points, the performance models are vectorized. When a model is vectorized, all the variables it contains become vectors, with each element corresponding to a different engine operating point. Figure 1 provides a visual representation of static and performance models.

IV. Model Derivation

Constraint derivation follows the general framework of the TASOPT turbofan model [4], with minor changes to facilitate the removal on the on-design/off-design distinction. TASOPT station numbering was adopted and is presented in Fig. 4. The model assumes a two-spool engine with two compressors and two turbines. The model can support a geared fan. Values of C_p and γ are assumed for each engine component and are presented in Table 1. Isentropic relations were used to model working fluid state changes across turbomachinery components, and a shaft power balance was enforced on both the low- and high-pressure shafts. Details of these models are discussed in Appendices A and B. Remaining submodels are described in the following subsections.

A. Combustor and Cooling Flow Mixing Model

The combustor and cooling flow constraints serve two purposes: to determine the fuel mass flow percentage and to account for the total pressure loss resulting from the mixing of the cooling flow and the working fluid in the main flow path. The flow mixing model is taken directly from TASOPT [4].

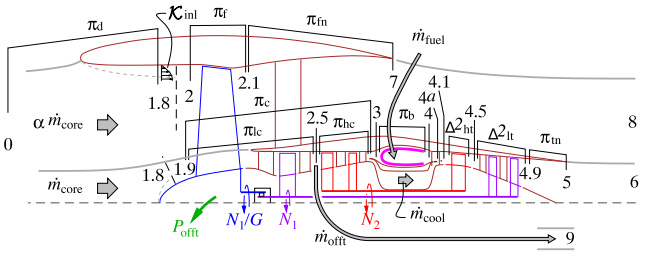

Fig. 4 TASOPT engine station numbering, which was adopted for this paper.

Table 1 Assumed gas properties for each engine component

Engine component	C_p, J/kg · K	γ	Corresponding air temperature, K
Diffuser	1005	1.4	260
LPC	1008	1.398	350
HPC	1099	1.354	800
Combustor	1216	1.313	1500
HPT	1190	1.318	1300
LPT	1142	1.335	1000
Core exhaust	1029	1.387	500
Fan exhaust	1005	1.4	273

The fuel mass flow and T_{t_4} are constrained via an enthalpy balance [Eq. (6)], whereas Eqs. (7, 8) determine the remaining station 4 states. η_b is the burner efficiency; a value less than 1 indicates a portion of injected fuel is not burned. The specified f_c is the cooling flow bypass ratio whose typical values range from 0.2 to 0.3, with lower values indicating a higher engine technology level. $C_{p_{\text{fuel}}}$ and h_f are taken as constants equal to 2010 J/kg · K and 43.003 MJ/kg, respectively. T_{t_f} is the fuel's temperature when injected into the combustor, and π_b is the combustor pressure ratio. Both are user inputs:

$$\eta_b f_f h_f \geq (1 - f_c)(h_{t_4} - h_{t_3}) + C_{p_{\text{fuel}}} f_f (T_{t_4} - T_{t_f}) \tag{6}$$

$$h_{t_4} = C_{p_c} T_{t_4} \tag{7}$$

$$P_{t_4} = \pi_b P_{t_3} \tag{8}$$

It is assumed the cooling flow is unregulated and engine pressure ratios are relatively constant, as such, f_c will not change between operating points. Further, it is assumed that the cooling flow is discharged entirely over the first row of inlet guide vanes (station 4a) and mixes completely with the main flow before the first row of turbine blades (station 4.1). The first row of inlet guide vanes requires the majority of the cooling flow, justifying this assumption.

The mixed out flow temperature at station 4.1 is computed with the enthalpy balance in Eq. (9). Note that this is a signomial equality:

$$h_{t_{4.1}} f_{f+1} = (1 - f_c + f_f) h_{t_4} + f_c h_{t_3} \tag{9}$$

The mixed-out state at station 4.1 is computed in terms of the temperature ratio Z_{4a}, which is introduced for GP compatibility:

$$Z_{4a} = 1 + \frac{1}{2}(\gamma - 1)(M_{4a})^2 \tag{10}$$

$$P_{4a} = P_{t_4} (Z_{4a})^{-(\gamma_i/(\gamma_i - 1))} \tag{11}$$

$$u_{4a} = M_{4a} \sqrt{\gamma_{4a} R T_{t_4} / Z_{4a}} \tag{12}$$

Cooling flow velocity u_{cool} is defined by the user-input cooling flow velocity ratio r_{uc}:

$$u_{\text{cool}} = r_{\text{uc}} u_{4a} \tag{13}$$

Static pressure rise during mixing is neglected and the station 4.1 state is computed using stagnation relations. Equation (15) is a signomial equality constraint:

$$P_{t_{4.1}} = P_{4a} \left(\frac{T_{t_{4.1}}}{T_{4.1}} \right)^{\gamma_i/(\gamma_i - 1)} \tag{14}$$

$$T_{4.1} = T_{t_{4.1}} - \frac{1}{2}\frac{{u_{4.1}}^2}{C_{p_c}} \tag{15}$$

Rather than introduce a full momentum balance, this model approximates $u_{4.1}$ as the geometric average of core and cooling flow velocities:

$$f_{f+1}u_{4.1} = \sqrt{f_{f+1}u_{4a}\alpha_{\text{cool}}u_{\text{cool}}} \tag{16}$$

B. Area, Mass Flow, and Speed Constraints

Either the engine's thrust or the turbine inlet temperature must be constrained via Eq. (17) or Eq. (18). In a full aircraft optimization problem, F_{spec} can be linked to thrust requirements in an aircraft performance model. When the engine model is run in isolation, F_{spec} or $T_{t_{4.1}}$ must be specified by the user:

$$F = F_{\text{spec}} \tag{17}$$

$$T_{t_{4.1}} = T_{t_{4_{\text{spec}}}} \tag{18}$$

Component speed ratios are determined by the turbomachinery maps (Sec. IV.C). Only the ratio of component speed to the component's nominal design speed is considered, and so the nominal design speed is arbitrarily set to 1. Thus, a low-pressure compressor (LPC) speed of $N_1 = 1.1$ should be thought of as an LPC speed 10% faster than the component's nominal design speed, not a value 10% over maximum rotational frequency. This model does not attempt to constrain actual rotational frequency values.

The fan and LPC both lie on the low-pressure shaft, and so their speeds are correlated via Eq. (19), which allows for a user-selected gearing ratio G_f. Additionally, a maximum allowable speed is set for the fan and compressors. The maximum speed of 1.1 is estimated from TASOPT output. If an upper bound is not placed on speed, the optimizer will indefinitely increase component speed to drive OPR higher. When solving across an engine mission profile, the upper speed bound will only be achieved at the engine's most demanding operating point:

$$N_f = G_f N_1 \tag{19}$$

$$N_1 \leq 1.1 \tag{20}$$

$$N_2 \leq 1.1 \tag{21}$$

Constraints on the mass flux through engine components are used to ensure that each engine operating point corresponds to an engine of the same physical size. The station 5 and 7 exit states are determined using user-specified nozzle pressure ratios as well as isentropic and stagnation relations:

$$P_{t_5} = \pi_{\text{tn}}P_{t_{4.9}} \tag{22}$$

$$P_{t_7} = \pi_{\text{fn}}P_{t_2} \tag{23}$$

$$P_i \geq P_0 \tag{24}$$

$$\frac{P_i}{P_{t_i}} = \left(\frac{T_i}{T_{t_i}}\right)^{\gamma/(\gamma-1)} \tag{25}$$

$$\left(\frac{T_i}{T_{t_i}}\right)^{-1} \geq 1 + 0.2(M_i)^2 \tag{26}$$

Equation (27) is a deviation from constraints in traditional engine models that use Newton's method or a comparable iterative procedure. In many methods, M_5 and M_7 are set equal to 1 if M_6 or M_8 is respectively greater than 1 so that the exit nozzle is choked. If M_6 or M_8 is less than 1, then M_5 and M_7 are constrained to be less than 1. A switch is used to change constraints midsolve. It is not possible to switch constraints during a GP solve. Therefore, M_5 and M_7 are constrained to be less than or equal to 1, regardless of M_6 and M_8. For the mild choking typical in efficient turbofans, the effects of this reformulation are negligible, as confirmed by Sec. V:

$$M_i \leq 1 \tag{27}$$

Equations (28–38) set A_2, $A_{2.5}$, A_5, and A_7. Note that $M_{2.5}$ is set by the user, and M_2 is either linked to an aircraft performance model or set by the user:

$$a_i = \sqrt{\gamma RT_i} \tag{28}$$

$$u_i = a_i M_i \tag{29}$$

$$\rho_i = \frac{P_i}{RT_i} \tag{30}$$

In the static property calculations, the temperature ratio Z_i is again introduced for GP compatibility:

$$Z_i = 1 + \frac{\gamma_i - 1}{2}M_i^2 \tag{31}$$

$$P_i = P_{t_i}(Z_i)^{\gamma_i/(1-\gamma_i)} \tag{32}$$

$$T_i = T_{t_i}Z_i^{-1} \tag{33}$$

$$h_i = C_{p_i}T_i \tag{34}$$

In Eq. (35), the value of $C_{p_i} - R$ is precomputed and substituted into the constraint to make it GP-compatible:

$$u_i = M_i\sqrt{C_{p_i}RT_i/(C_{p_i} - R)} \tag{35}$$

$$\dot{m}_{\text{fan}} = \rho_7 A_7 u_7 \tag{36}$$

$$\dot{m}_{\text{core}}\bar{f}_o = \rho_5 A_5 u_5/f_{f+1} \tag{37}$$

$$\alpha = \dot{m}_{\text{fan}}/\dot{m}_{\text{core}} \tag{38}$$

Full turbine maps are not used to constrain turbine mass flow. Instead, it is assumed that the entry to each turbine is always choked. This leads to two constraints, each setting the corrected mass flow at turbine entry equal to the estimated nominal value:

$$\bar{m}_{\text{HPT}_D} = \bar{m}_{\text{HPC}}f_{f+1}\bar{f}_o(P_{t_{2.5}}/P_{t_{4.1}})\sqrt{T_{t_{4.1}}/T_{t_{2.5}}} \tag{39}$$

$$\bar{m}_{\text{LPT}_D} = \bar{m}_{\text{LPC}}f_{f+1}\bar{f}_o(P_{t_{1.8}}/P_{t_{4.5}})\sqrt{T_{t_{4.5}}/T_{t_{1.8}}} \tag{40}$$

The optimized nominal core mass flow is computed via Eq. (41). $\hat{T}_i$ and $\hat{P}_i$ represent the estimated nominal state at engine station i. The values of $\hat{T}_{t_4}$, $\hat{P}_{t_2}$, and $\hat{T}_{t_2}$ are set by the user, whereas all other $\hat{T}$ and $\hat{P}$ values are estimated using the isentropic relations, component

Downloaded by MASSACHUSETTS INST OF TECHNOLOGY on November 24, 2017 | http://arc.aiaa.org | DOI: 10.2514/1.C034463

Downloaded by MASSACHUSETTS INST OF TECHNOLOGY on November 24, 2017 | http://arc.aiaa.org | DOI: 10.2514/1.C034463

design pressure ratios, and a shaft power balance. This process is shown in Eq. (42). Nominal mass flows are allowed to vary plus or minus 30% from their estimated values to account for uncertainty in the estimation process and ensure that, if the nominal design condition is estimated to occur at the aircraft's average altitude, the optimizer can place the nominal state anywhere in the flight. Optimization of the nominal state enables removal of the a priori specification of an engine on-design point:

$$\bar{m}_{\text{component}_D} \le 1.3 f_{f+1} \bar{f}_o \dot{m}_{\text{core}_D} \sqrt{\hat{T}_{t_i}/T_{\text{ref}}}/(\hat{P}_{t_i}/P_{\text{ref}})$$
$$\bar{m}_{\text{component}_D} \ge 0.7 f_{f+1} \bar{f}_o \dot{m}_{\text{core}_D} \sqrt{\hat{T}_{t_i}/T_{\text{ref}}}/(\hat{P}_{t_i}/P_{\text{ref}}) \qquad (41)$$

$$\begin{aligned}
\hat{P}_i &= \pi_{\text{component}} \hat{P}_{i-1} \\
\hat{T}_{t_i} &= \hat{T}_{t_{i-1}} (\pi_{\text{component}})^{(\gamma_i - 1)/\gamma_i \eta_i} \\
\hat{T}_{t_{4.5}} &= \hat{T}_{t_{4.1}} - (\hat{T}_{t_3} - \hat{T}_{t_{2.5}}) \\
\hat{T}_{t_{4.9}} &= \hat{T}_{t_{4.5}} - (\hat{T}_{t_{2.5}} - \hat{T}_{t_{2.1}}) \\
\hat{\pi}_{\text{HPT}} &= \left(\frac{\hat{T}_{t_{4.5}}}{\hat{T}_{t_{4.1}}} \right)^{\eta_i \gamma/(\gamma-1)} \\
\hat{P}_{t_{4.5}} &= \hat{\pi}_{\text{HPT}} \hat{P}_{t_3}
\end{aligned} \qquad (42)$$

C. Fan and Compressor Maps

Fan and compressor maps are required to accurately constrain fan and compressor pressure ratios. Every engine has different compressor maps that result from detailed turbomachinery design. The present model does not attempt to take into account factors causing variations in turbomachinery maps. Instead, a simple compressor and fan map is assumed and applied to all engines. As argued in Sec. V, this is accurate enough for aircraft conceptual design optimization.

GP-compatible fan and compressor maps were derived from NASA's Energy Efficient Engine (E3) program [13] turbomachinery maps, which are presented in Figs. 5 and 6. These are also the maps used in TASOPT. Solid curves are lines of constant component speed, and dashed curves are the estimated engine operating line, or spine. Each spine can be parameterized as either $\pi = f(\bar{m})$ or $\pi = f(N)$, where $\bar{m}$ is normalized corrected mass flow, and N is component speed. The normalized corrected mass flow for each components is defined next:

$$\bar{m}_{\text{HPC}} = \dot{m}_{\text{core}} \sqrt{T_{t_{2.5}}/T_{\text{ref}}}/(P_{t_{2.5}}/P_{\text{ref}}) \qquad (43)$$

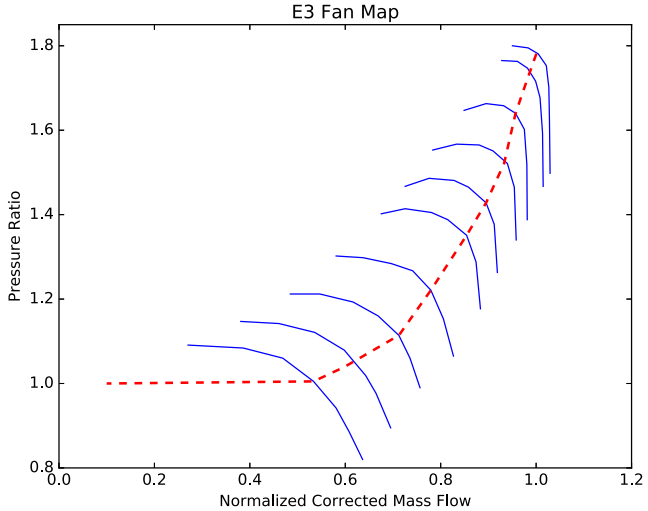

Fig. 5 E3 fan map with a design pressure ratio of 1.7. The dashed line is the estimated engine operating line.

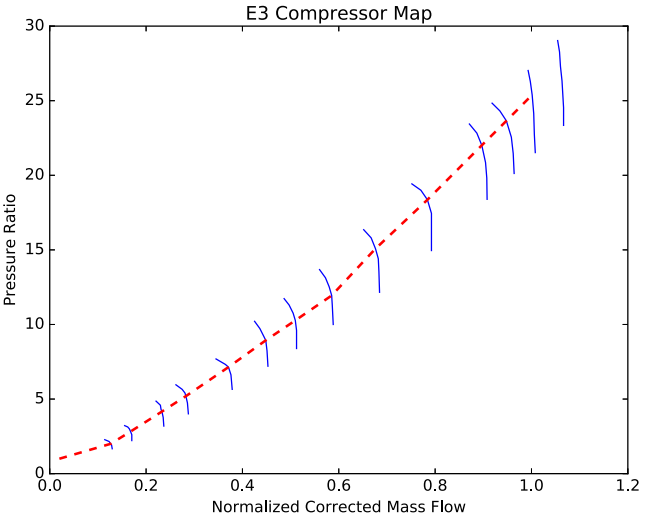

Fig. 6 E3 compressor map with a design pressure ratio of 26. The dashed line is the estimated engine operating line.

$$\bar{m}_{\text{LPC}} = \dot{m}_{\text{core}} \sqrt{T_{t_2}/T_{\text{ref}}}/(P_{t_2}/P_{\text{ref}}) \qquad (44)$$

$$\bar{m}_{\text{fan}} = \dot{m}_{\text{fan}} \sqrt{T_{t_2}/T_{\text{ref}}}/(P_{t_2}/P_{\text{ref}}) \qquad (45)$$

A GP-compatible monomial approximation to the functions $\pi = f(\bar{m})$ and $\pi = f(N)$ was developed with GPfit [14,15]. The approximations for both the compressor and fan map spine fits are given by Eqs. (46–49) and plotted in Figs. 7 and 8:

$$\pi_{\text{comp}} = 20.1066(N)^{5.66} \qquad (46)$$

$$\pi_{\text{comp}} = 25.049(\bar{m})^{1.22} \qquad (47)$$

$$\pi_{\text{fan}} = 1.6289(N_f)^{0.871} \qquad (48)$$

$$\pi_{\text{fan}} = 1.7908(\bar{m})^{1.37} \qquad (49)$$

The fan map spine was only fit for speeds greater than 0.6. Single term fits are monomials that must pass through the origin, limiting their ability to capture fan trends for low speeds. During a typical flight, the low-pressure spool speed (N_1) will rarely, if ever, drop below 0.6. The fitted map, combined with the constraint that all pressure ratios are greater than 1, places an implicit lower bound on N_1 and N_f, which may lead to modeling inaccuracy at low throttle settings. This is acceptable due to the proportionally small amount of fuel burned at low throttle settings. A two-term polynomial fit yields a better approximation of the fan map but was not used because it adds an additional signomial constraint.

Equations (50–52) are fan and compressor map approximations obtained by scaling the E3 map fits to an arbitrary design pressure ratio and constraining the pressure ratio be within 10% of the spine mass flow fit. This allows the operating point to move off the operating line while ensuring that the operating point does not move into either the stall or surge regime. The user must specify, at a minimum, either fan, LPC, and high-pressure compressor (HPC) design pressure ratios or a maximum turbine inlet temperature $T_{t_{4.1}}$. The user may specify all four values. Setting fan, LPC, and HPC design pressure ratios values scales the maps and is distinct from specifying a full engine on-design operating point. If component design pressure ratios are left free, a maximum turbine inlet temperature must be specified so that the cooling model prevents OPR from being driven to infinity:

Downloaded by MASSACHUSETTS INST OF TECHNOLOGY on November 24, 2017 | http://arc.aiaa.org | DOI: 10.2514/1.C034463

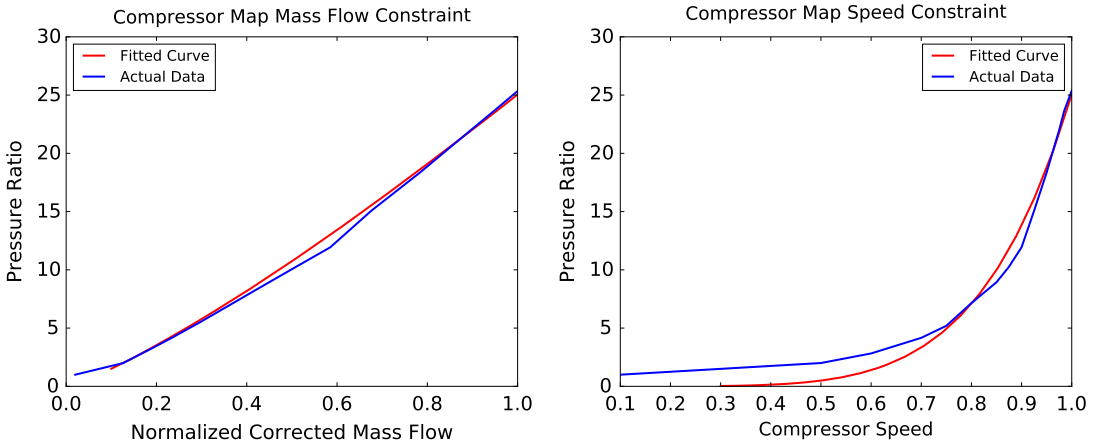

a) Mass flow parametrization **b) Speed parametrization**

Fig. 7 Monomial approximations to the E3 compressor map spine.

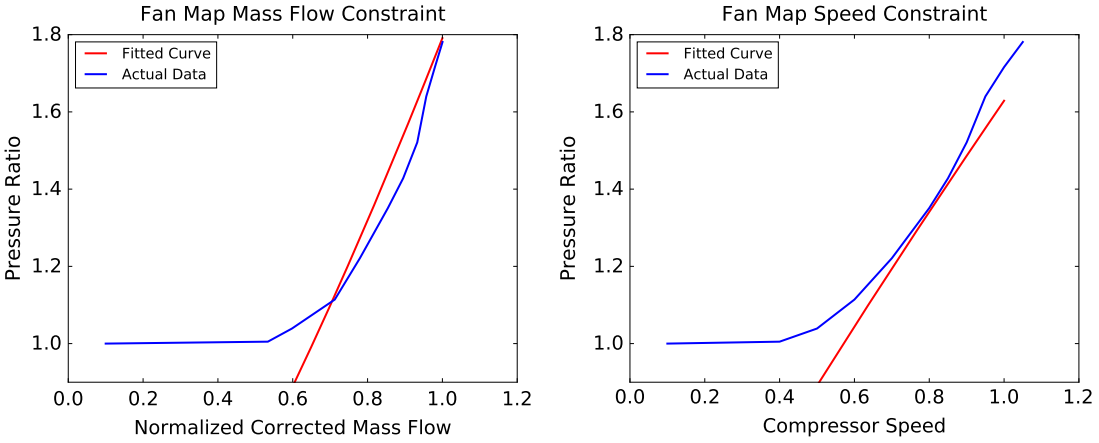

a) Mass flow parametrization **b) Speed parametrization**

Fig. 8 Monomial approximations to the E3 fan map spine.

$$\pi_{\text{fan}}\left(\frac{1.7}{\pi_{f_D}}\right) = 1.6289(N_f)^{0.871}$$
$$\pi_{\text{fan}}\left(\frac{1.7}{\pi_{f_D}}\right) \geq (0.9)(\bar{m}_f)^{1.37}$$
$$\pi_{\text{fan}}\left(\frac{1.7}{\pi_{f_D}}\right) \leq (1.1)(\bar{m}_f)^{1.37} \tag{50}$$

$$\pi_{\text{LPC}}\left(\frac{26}{\pi_{\text{LPC}_D}}\right) = 20.1066(N_1)^{5.66}$$
$$\pi_{\text{LPC}}\left(\frac{26}{\pi_{rm\text{LPC}_D}}\right) \geq (0.9)25.049(\bar{m}_{\text{LPC}})^{1.22}$$
$$\pi_{\text{LPC}}\left(\frac{26}{\pi_{rm\text{LPC}_D}}\right) \leq (1.1)25.049(\bar{m}_{\text{LPC}})^{1.22} \tag{51}$$

$$\pi_{\text{HPC}}\left(\frac{26}{\pi_{\text{HPC}_D}}\right) = 20.1066(N_2)^{5.66}$$
$$\pi_{\text{HPC}}\left(\frac{26}{\pi_{\text{HPC}_D}}\right) \geq (0.9)25.049(\bar{m}_{\text{HPC}})^{1.22}$$
$$\pi_{\text{HPC}}\left(\frac{26}{\pi_{\text{HPC}_D}}\right) \leq (1.1)25.049(\bar{m}_{\text{HPC}})^{1.22} \tag{52}$$

It is possible to fit a full fan/compressor map instead of just the spine. However, there is no way to distinguish valid map points from points in the surge/stall regime. The optimizer will push the operating point toward these sections of the map, resulting in a physically invalid solution. This work employs the TASOPT assumption that fan and compressor operating lines are fixed throughout a flight. The accuracy of this approximation decreases as FPR decreases.

D. Exhaust State Model

Thrust is determined with a momentum balance. Station 6 (core exhaust) and 8 (fan exhaust) velocities are computed by Eqs. (53–57), which employ the stagnation relations and assume isentropic flow expansion:

$$\left(\frac{P_i}{P_{t_i}}\right)^{(\gamma_i-1)/\gamma_i} = \frac{T_i}{T_{t_i}} \tag{53}$$

$$P_i = P_0 \tag{54}$$

$$h_{t_i} = C_{p_i} T_{t_i} \tag{55}$$

$$h_i = C_{p_i} T_i \tag{56}$$

$$u_i^2 + 2h_i \leq 2h_{t_i} \tag{57}$$

Downloaded by MASSACHUSETTS INST OF TECHNOLOGY on November 24, 2017 | http://arc.aiaa.org | DOI: 10.2514/1.C034463

Fan and core thrust (F_8 and F_6) are computed with a momentum balance and summed to set the total thrust:

$$F_8/(\alpha\dot{m}_{\text{core}}) + u_0 \le u_8 \tag{58}$$

$$F_6/(\bar{f}_o\dot{m}_{\text{core}}) + u_0 \le u_6 \tag{59}$$

$$F \le F_6 + F_8 \tag{60}$$

The specific thrust and corresponding thrust-specific fuel consumption then follow:

$$F_{\text{sp}} = F/(a_0\alpha_{+1}\dot{m}_{\text{core}}) \tag{61}$$

$$\text{TSFC} = \frac{f_f g}{F_{\text{sp}} a_0 \alpha_{+1}} \tag{62}$$

The preceding thrust derivation assumes a convergent divergent nozzle. If a convergent only nozzle is desired, the core thrust constraint becomes $F_5/(\bar{f}_o\dot{m}_{\text{core}}) + u_0 \le u_5 + (P_5 - P_0)A_5/(\bar{f}_o\dot{m}_{\text{core}})$, and the fan thrust constraint becomes $F_7/(\alpha\dot{m}_{\text{core}}) + u_0 \le u_7 + (P_7 - P_0)A_7/(\bar{f}_o\dot{m}_{\text{core}})$. Both of these constraints are signomials. To minimize solution speed, the remainder of this work assumes a convergent divergent nozzle (generally minimizing the number of signomial constraints minimizes solution speed). When comparing to a purely convergent nozzle, this can result in optimistic thrust values, but as demonstrated in Sec. V, the effect is small.

E. Engine Weight

In aircraft optimization problems there is a downward pressure on engine weight. Consequently, the TASOPT [4] engine weight model can be relaxed into a posynomial inequality constraint. The TASOPT engine weight model is a fit to production engine data and does not account for the weight of a gearbox in a geared turbofan. The GP-compatible engine mass constraint, taken from TASOPT [4], is presented next. $\dot{m}_{\text{total}}$ is defined by Eq. (64):

$$m_{\text{engine}} \ge \frac{\dot{m}_{\text{total}}}{(100\ \text{lbm/s})\alpha_{+1}}\left(1684.5\ \text{lbm} + 17.7\ \text{lbm}\frac{\pi_f\pi_{\text{LPC}}\pi_{\text{HPC}}}{30} + 1662.2\ \text{lbm}\left(\frac{\alpha}{5}\right)^{1.2}\right) \tag{63}$$

$\dot{m}_{\text{core}}$ is written in the equivalent form $\dot{m}_{\text{total}}/\alpha_{+1}$, as such, an increase in either core or fan mass flow corresponds to an increase in engine weight. This formulation places the required downward pressure on both fan and core mass flows:

$$\dot{m}_{\text{total}} \ge \dot{m}_{\text{core}} + \dot{m}_{\text{fan}} \tag{64}$$

V. Model Validation

The presented model was validated against the output of a CFM56-7B27-like NPSS model, a GE90-94B-like NPSS model, and TASOPT. The NPSS models were developed by Georgia Tech with publicly available data under the FAA's Environmental Design Space effort [16]. The TASOPT data was taken from a 737-800 optimization run. The TASOPT engine output should mirror that of Georgia Tech's CFM56-like model because the CFM56-7B family powers all 737 Next Gen aircraft [17]. The intent of the validation studies was to verify the model's physics modeling, not to find the most optimal engine. Essentially, during validation, the model was used for engine analysis instead of optimization.

In all validation cases, bypass ratio (BPR) was constrained to be less than the validation data's maximum BPR. This prevents BPR from growing without bound. During validation, the objective function was the sum of all climb TSFCs plus 10 times the cruise TSFC. Cruise TSFC was weighted by a factor of 10 to capture the fact that a commercial aircraft spends the majority of each flight in cruise. Optimizing TSFC does not apply a downward pressure to engine weight. Thus, engine weight was capped at the simulated engine's predicted/actual engine weight:

$$\text{objective} = \sum \text{TSFC}_{\text{climb}} + 10\text{TSFC}_{\text{cruise}} \tag{65}$$

Component polytropic efficiencies, duct pressure losses, cooling flow bypass ratio, and maximum BPR are estimated from TASOPT/NPSS output. To mitigate errors due to the SP model's assumed gas properties, TASOPT-computed turbine C_p values were used in all three validation cases (NPSS computed C_p was not available in the provided output). These values, along with the assumed fuel temperature, are presented in Table 2.

Validation solution speeds are presented in Table 3.

A. Numerical Propulsion System Simulation CFM56 Validation

The SP model's input values are given in Table 4. The SP model was constrained by two operating points, on-design and top of climb (TOC), detailed in Table 5. The cruise and TOC operating points have similar ambient conditions and thrust requirements. The SP model should place the on-design point near the NPSS on-design point, producing little variation in predicted TSFC. Validation results are given in Table 6.

Table 2 Input values used in all three validation cases

Variable	Value
T_{t_f}	435 K
$C_{p_{4.1}}$	1.280 KJ/(kg · K)
$C_{p_{4.5}}$	1.184 KJ/(kg · K)

Table 3 Number of GP solves and solution time for each validation case

Validation case	Number of GP solves	Solution time, s
CFM56	7	0.61
TASOPT	7	0.81
GE90	7	0.78

Table 4 Input values used for CFM56 engine validation

Variable	Value	Variable	Value
π_{f_D}	1.685	$\alpha_{\max}$	5.105
π_{LPC_D}	1.935	f_c	0.19036
π_{HPC_D}	9.369	η_{fan}	0.9005
η_b	0.9827	η_{LPC}	0.9306
G_f	1	η_{HPC}	0.9030
$\bar{f}_o$	0.9556	η_{HPT}	0.9030
η_{LPT}	0.8851	$\eta_{\text{HP}}, \eta_{\text{LP}}$	0.97
π_{tn}	0.98	π_b	0.94
π_d	0.98	π_{fn}	0.98
W_{engine}	23,201 N	— —	— —

Table 5 The two operating points used during CFM56 validation

Flight condition	Altitude, ft	Mach number	Thrust, lbf
TOC	35,000	0.8	5961.9
On-design (cruise)	35,000	0.8	5496.4

Downloaded by MASSACHUSETTS INST OF TECHNOLOGY on November 24, 2017 | http://arc.aiaa.org | DOI: 10.2514/1.C034463

Table 6 NPSS CFM56 validation results, expected to be similar when $h_f = 40.8$ MJ/kg

Flight condition	Predicted TSFC, 1/h	NPSS TSFC, 1/h	Percent difference, %
On-design (SP $h_f = 43.003$ MJ/kg)	0.6335	0.6793	−6.74
On-design (SP $h_f = 40.8$ MJ/kg)	0.6679	0.6793	−1.68
Top of climb (SP $h_f = 43.003$ MJ/kg)	0.6431	0.6941	−7.34
Top of climb (SP $h_f = 40.8$ MJ/kg)	0.6780	0.6941	−2.31
TASOPT on-design (implied $h_f = 42.68$ MJ/kg)	0.63403	0.6941	−6.66

The SP turbofan model was solved for two different h_f values. Typically, the SP model has an h_f of 43.003 MJ/kg. However, Georgia Tech's NPSS model has an implied h_f value of 40.8 MJ/kg, 5.12% less than SP model's value and 2 MJ/kg below the minimum h_f of jet A [18]. Solving the SP model with an h_f of 40.8 MJ/kg reduces the percent error at each operating point by approximately 5%. The remaining error can be accounted for by variations in component maps and gas properties as well as the convergent divergent nozzle assumption.

B. Transport Aircraft System Optimization Validation

The SP turbofan model was validated against three TASOPT operating points: takeoff, TOC, and on-design. The parameters for each operating point are given in Table 7. The constant input values are given in Table 8. Limiting the SP engine weight to the TASOPT engine weight results in TSFC errors of 10.6, 18.0, and 7.9% at takeoff, TOC, and the on-design point (cruise), respectively. This error results from the engine weight constraint [Eq. (63)] as well as the fan and compressor maps (Sec. IV.C), which set the component pressure ratios, placing an implicit upper bound on engine mass flow. At the on-design point, the SP engine has a core mass flow 15.6% lower than the TASOPT engine. To match the TASOPT engine's thrust, the SP engine must impart a larger velocity change to the working fluid; this increases TSFC. TASOPT [4] uses an approximation different from the E3 fan and compressor maps that allow its engines to achieve a greater mass flow for a given engine weight.

If the SP engine weight is instead capped at 110% of the TASOPT engine weight, the mass flow discrepancy is reduced to 0.1%. The TSFC errors for this case are presented in in Table 9. Note that the on-design TSFC error is now less than 1%. No matter the cap on engine weight, the greatest TSFC error occurs at the TOC condition. At TOC, the low-pressure spool is at its maximum allowed speed of 1.1. As discussed in Sec. IV.C, the SP model's fan map is conservative, particularly for high fan speeds. At a spool speed of 1.1, the SP model predicts an FPR of 1.75, whereas TASOPT has an FPR of 1.87, 6.28% higher. The SP model's lower FPR causes the engine to produce more core thrust, lowering efficiency and increasing TSFC.

Table 7 The three operating points used when validating the presented model against TASOPT

Flight condition	Altitude, ft	Mach number	Thrust, lbf
Takeoff	0	0.223	21,350
TOC	35,000	0.8	6,768
On-design (cruise)	35,000	0.8	4,986

Table 8 Input values used for TASOPT engine validation

Variable	Value	Variable	Value
π_{f_D}	1.685	$\alpha_{\max}$	5.103
π_{LPC_D}	4.744	f_c	0.19036
π_{HPC_D}	3.75	η_{fan}	0.8948
η_b	0.985	η_{LPC}	0.88
G_f	1	η_{HPC}	0.87
$\bar{f}_o$	0.972	η_{HPT}	0.899
η_{LPT}	0.889	$\eta_{\mathrm{HP}}, \eta_{\mathrm{LP}}$	0.97
π_{tn}	0.989	π_b	0.94
π_d	0.998	π_{fn}	0.98
W_{engine}	35,008 N	— —	— —

Table 9 TASOPT validation results with engine weight capped at 110% of the TASOPT value, expected to be similar at on design

Flight condition	Predicted TSFC, 1/h	TASOPT TSFC, 1/h	Percent difference, %
Takeoff	0.4751	0.48434	−1.91
Top of climb	0.7166	0.65290	9.76
On design	0.6445	0.6404	0.69

C. Numerical Propulsion System Simulation GE90 Validation

The two operating points used for GE90 validation are given in Table 10. Again, TOC conditions are similar to cruise conditions so

Table 10 The two operating points used when validating the presented model against the GE90 like NPSS model

Flight condition	Altitude, ft	Mach number	Thrust, lbf
TOC	35,000	0.85	19,600
On-design (cruise)	35,000	0.8	16,408.4

Table 11 Input values used for GE90 engine validation

Variable	Value	Variable	Value
π_{f_D}	1.58	$\alpha_{\max}$	8.7877
π_{LPC_D}	1.26	f_c	0.1444
π_{HPC_D}	20.033	η_{fan}	0.9153
η_b	0.997	η_{LPC}	0.9037
G_f	1	η_{HPC}	0.9247
$\bar{f}_o$	0.955	η_{HPT}	0.9121
η_{LPT}	0.9228	$\eta_{\mathrm{HP}}, \eta_{\mathrm{LP}}$	0.97
π_{tn}	0.98	π_b	0.94
π_d	0.98	π_{fn}	0.98
W_{engine}	77,399 N	— —	— —

Table 12 NPSS GE90 validation results, expected to be similar at both operating points

Flight condition	Predicted TSFC, 1/h	NPSS TSFC, 1/h	Percent difference, %
On design	0.5328	0.5418	−1.66
TOC	0.5997	0.5876	2.59

Table 13 Aircraft sizing and flight profile inputs

Variable	Value
N_{eng}	2
$W_{S_{\max}}$	6664 N/m^2
e	0.9
$AR_{\max}$	10

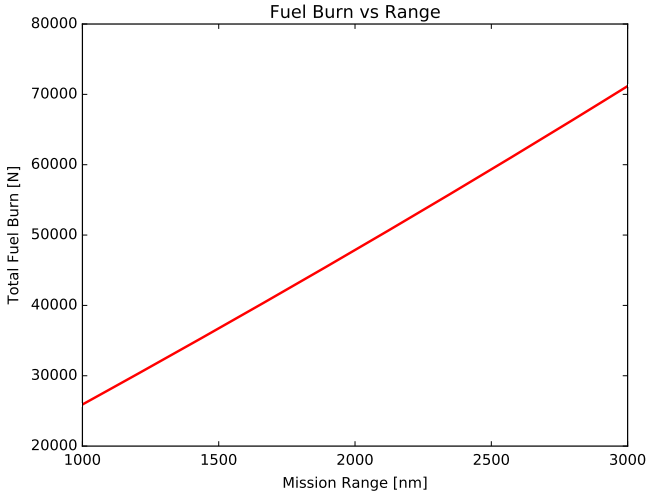

Fig. 9 Total fuel burn vs mission range.

TSFC discrepancies should be small. The SP model's input values are given in Table 11, and results are presented in Table 12. TSFC errors are due to assumed gas properties, variations in component maps, and the convergent divergent nozzle assumption. This validation case demonstrates that the presented model accurately scales from a CFM56 up to a GE90.

VI. Optimum-Aircraft Parametric Studies

The engine model was integrated with a simplified commercial aircraft sizing model, and the combined models were solved to find the aircraft/engine combination that burns the least amount of fuel. The model was solved with a variety of flight profiles as well as a varying number of missions, mission ranges, and minimum climb rates. Effects of these changes on engine sizing and parameter sensitivities are presented. The commercial aircraft sizing model is intentionally simple, capturing only general trends in aircraft sizing. A detailed description of the commercial sizing model is available in Appendix C. For the purposes of this paper, each mission was discretized into four flight segments: two climb and two cruise. The objective is to minimize total fuel burn. Table 13 lists the input values given to the aircraft model. The same engine input values are used as during CFM56 validation (Table 4), with the exception of maximum BPR. Maximum BPR was increased to 5.6958, the maximum value from the takeoff, climb, and cruise segments of a TASOPT 737-800 mission. The integrated engine/commercial aircraft sizing model has 628 free variables and solves in 6.78 s and six GP iterations.

A. Optimum-Aircraft Sensitivity to Specified Mission Range

To demonstrate that the combined model captures the proper trends, it was solved for a variety of mission ranges. Each point on the following plots represents a unique aircraft/engine combination. Total fuel burn increased with range, as shown by Fig. 9.

Figure 10 presents plots of maximum engine thrust, fan and core thrust, initial climb and cruise TSFC, and engine weight versus mission range. All values remain roughly constant across mission range.

B. Optimum-Aircraft Sensitivity to Specified Minimum Climb Rate

A minimum initial climb rate constraint was added to shift the nominal design point toward climb. The minimum climb rate was for normal operating conditions (i.e., both engines operating nominally). Increasing the minimum initial climb rate creates a need for increased thrust at low altitude, similar to adding a minimum balanced field

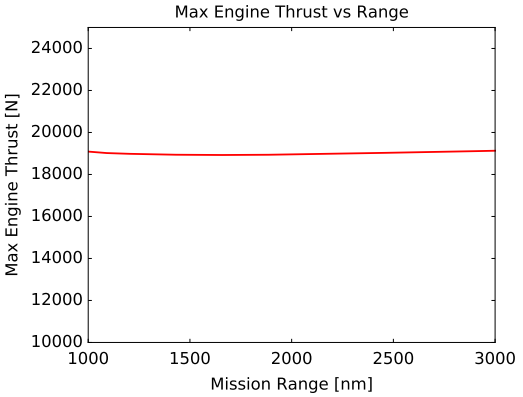

a) Max engine thrust, which occurs during the initial climb segment, versus mission range

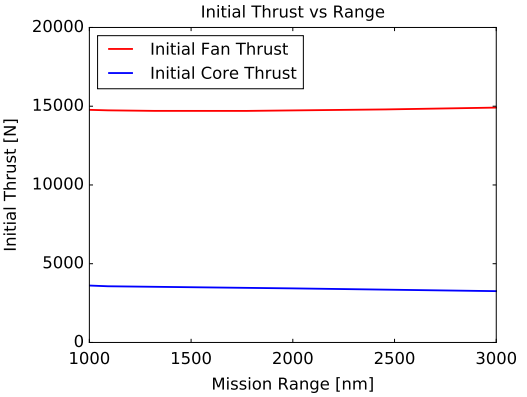

b) Fan and core thrust during the initial climb segment versus mission range

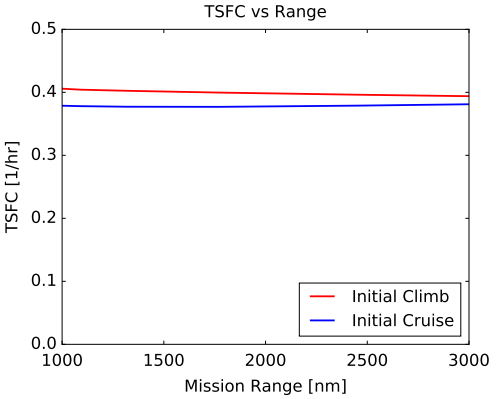

c) Initial climb and cruise TSFC versus mission range

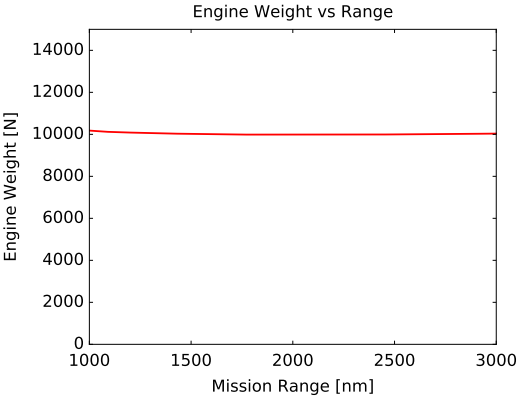

d) Engine weight versus mission range

Fig. 10 Initial engine thrust, core and fan thrust, climb and cruise TSFC, and engine weight for a variety of mission ranges.

Downloaded by MASSACHUSETTS INST OF TECHNOLOGY on November 24, 2017 | http://arc.aiaa.org | DOI: 10.2514/1.C034463

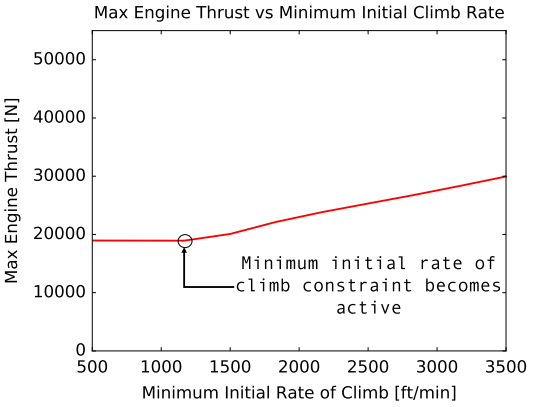

a) Total initial thrust

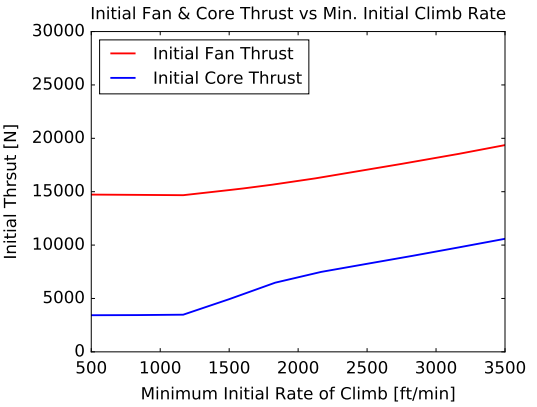

b) Initial fan and core thrust

Fig. 11 Initial fan and core thrust vs minimum initial climb rate.

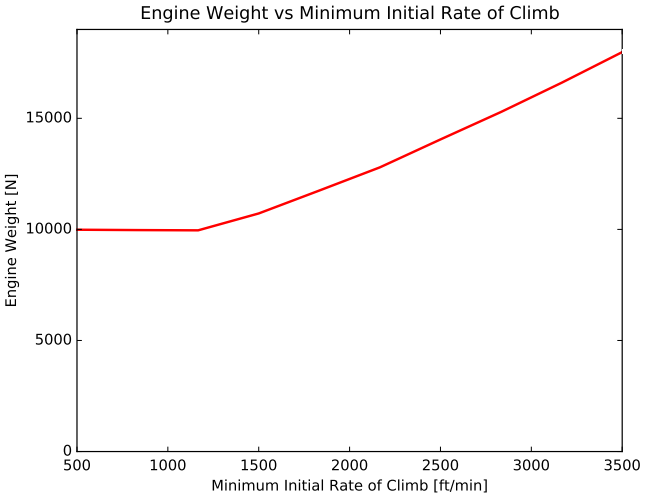

Fig. 12 Engine weight vs minimum initial climb rate.

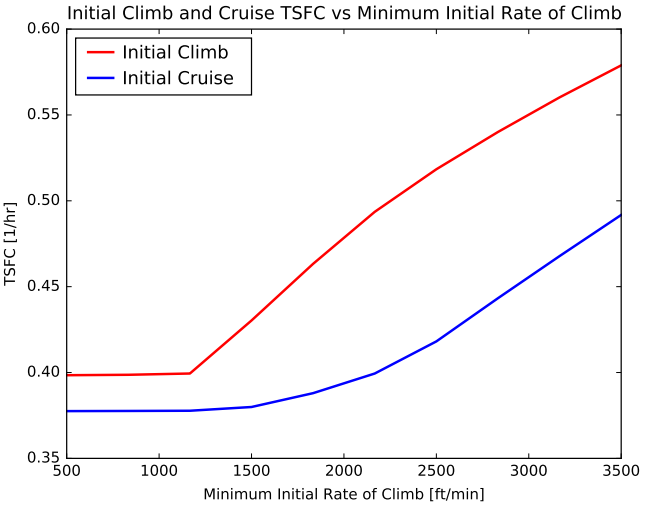

Fig. 14 Initial climb and cruise TSFC vs minimum initial climb rate.

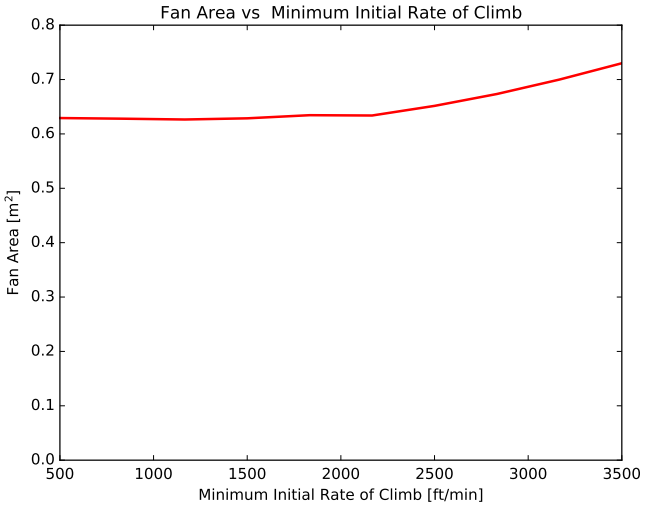

Fig. 13 Fan inlet area (A_2) vs minimum initial climb rate.

length requirement to an aircraft. The aircraft model was solved across a range of minimum climb rates.

The initial thrust requirement on the engine was larger the higher the minimum climb rate. This is presented in Fig. 11. The minimum climb rate constraint does not become active until the minimum climb rate exceeds 1170 ft/ min (creating a slope change on Figs. 11–14 at the point RC = 1170 ft/ min). The total thrust, fan thrust, and core thrust (also plotted in Fig. 11) all increase in a near linear manner.

The engine model predicts engine weight will increase with minimum rate of climb, as shown in Fig. 12. This is the same as saying that engine weight will increase with thrust, which is expected.

As the engine is required to produce more thrust, it gets physically larger. Figure 13 illustrates this with a plot of fan area versus minimum initial climb rate.

Figure 14 presents the initial climb and cruise TSFC versus the minimum initial climb rate. For low minimum initial climb rates, the nominal design point remained at cruise and the cruise TSFC was virtually unaffected by the higher climb rate. However, as the climb rate continued to increase, the design point shifted toward climb, and cruise TSFC began to increase. Essentially, the high minimum climb rate requirement is degrading cruise performance. A short balanced field length requirement would degrade the performance of a commercial aircraft in a similar way.

C. Full Mission Versus Cruise-Only Optimization

To illustrate how the removal of the on/off design point distinction allows this paper's engine model to select the optimal engine, the climb portion of the flight was removed, and the optimal cruise engine was compared to the full mission optimal engine. The aircraft in both missions had the same fuselage area, carried the same payload, and had a cruise range of 2000 n mile. Results are presented in Table 14. The nominal design point is shifted toward climb for the full mission engine,

Downloaded by MASSACHUSETTS INST OF TECHNOLOGY on November 24, 2017 | http://arc.aiaa.org | DOI: 10.2514/1.C034463

Downloaded by MASSACHUSETTS INST OF TECHNOLOGY on November 24, 2017 | http://arc.aiaa.org | DOI: 10.2514/1.C034463

Table 14 Differences in engine size when accounting for the full mission profile and just cruise

Variable	Full mission value	Cruise-only value	Percent difference, %
A_2	0.629 m^2	0.767 m^2	−21.88
A_5	0.205 m^2	0.232 m^2	−13.12
A_7	0.391 m^2	0.472 m^2	−20.65
Engine weight	9,985.1 N	5,870.4 N	41.21
Initial cruise TSFC	0.378 1/h	0.381 1/h	−1.19

Table 15 Differences in engine size for the presented multimission optimization formulation and a single 2000 n mile range mission optimization

Variable	Single mission value	Multimission value	Percent difference, %
A_2	0.629 m^2	0.626 m^2	0.47
A_5	0.205 m^2	0.214 m^2	−3.97
A_7	0.391 m^2	0.403 m^2	−3.17
Engine weight	9,985.1 N	10,178.0 N	−1.93
2000 n mile fuel burn	47,870 N	48,076 N	−0.43

Table 16 Top engine design value sensitivities in the aircraft optimization example for a single 2000 n mile mission

Symbol	Description	Sensitivity
$\bar{f}_o$	1 minus percent mass flow bled	−2.50
η_{HPshaft}	High-pressure shaft power transmission efficiency	−1.50
π_d	Diffuser pressure ratio	−1.40
η_b	Combustor efficiency	−1.10
π_{fn}	Fan duct pressure loss	−1.00
η_{LPshaft}	Low-pressure shaft power transmission efficiency	−0.86
π_b	Burner pressure ratio	−0.39
π_{f_D}	On-design fan pressure ratio	0.53

Table 17 Top aircraft design and mission parameter sensitivities in the aircraft optimization example

Variable	Description	Sensitivity
e	Oswald efficiency factor	−0.45
W_{pax}	Passenger weight	0.65
Rng	Required range	0.94

causing it to burn 3.37% more fuel during cruise than the cruise-only engine. All component areas are larger on the cruise-only engine, which is (surprisingly) also 41% lighter. When climb is not considered, the maximum thrust requirement and mass flow through the engine are substantially smaller. Consequently, the mass flow dependent data fit engine weight model (Sec. IV.E) predicts an unrealistically light engine.

D. Multimission Optimization

An extra layer of vectorization was added, and the presented engine and simple aircraft model was simultaneously optimized across four missions of ranges 500, 1000, 1500, and 2000 n mile. Commercial aircraft are designed for high mission flexibility, which degrades overall fuel efficiency, motivating the use of multiple design reference missions when optimizing an aircraft [19]. For simplicity, payload remained constant for each mission. It is assumed that the aircraft being optimized will fly 500 n mile missions 37.5% of the time, 1000 n mile mission 37.5% of the time, 1500 n mile missions 12.5% of the time, and 2000 n mile missions 12.5% of the time. Equation (66) is the weighted objective function for this problem:

$$\text{objective} = 0.375W_{\text{fuel}_{500\,\text{nm}}} + 0.375W_{\text{fuel}_{1,000\,\text{nm}}} + 0.125W_{\text{fuel}_{1,500\,\text{nm}}} + 0.125W_{\text{fuel}_{2,000\,\text{nm}}} \tag{66}$$

Table 15 presents differences in the optimal engine size and fuel burn for the two optimizations. As expected, the multimission optimized aircraft burns more fuel during the 2000 n mile mission than the aircraft optimized for just the 2000 n mile flight.

The multimission optimization problem has 2480 free variables and takes 3.71 s and six GP iterations to solve.

E. Sensitivity Discussion

A strength of convex optimization is that, together with the optimum solution, it provides sensitivities of this solution to all model parameter values. Sensitivities are all local and computed about the optimal point. Equation (67) [10] is the formula for parameter sensitivities. If the sensitivity to a constant is 0.5, then decreasing that constant by 1% will decrease the objective by approximately one half of a percent. If the sensitivity to a constant is −0.75, then a 1% increase in the constant will decrease the objective by approximately three quarters of a percent. Analyzing a model's sensitivities can be useful in two ways. The first is to determine which areas of a physical design should be improved. For example, if the sensitivity to burner pressure drop is very large, it is advantageous to make the burner pressure drop as small as possible. The second way sensitivities can be used is to guide model development. If the sensitivity to a constant is low, it may not be worthwhile to develop an intricate model for that constant. However, if the sensitivity is large, it is important to ensure it is accurately modeled:

$$\text{Parameter Sensitivity} = \frac{\text{Fractional Objective Function Change}}{\text{Fractional Parameter Change}} \tag{67}$$

The integrated aircraft optimization problem was solved with a mission range of 2000 n mile. Table 16 presents a subset of engine sensitivities. The solution is most sensitive to core bleed flow, high-pressure shaft power transmission efficiency, diffuser pressure ratio, combustor efficiency, and the fan duct pressure loss. Increasing any of these values will decrease fuel burn. There is a positive sensitivity to the fan design pressure ratio. Decreasing the fan design pressure ratio will decrease fuel burn.

Table 17 presents sensitivities to some of the assumed constants in the aircraft model. Trends are as expected. Increasing the Oswald efficiency factor decreases fuel burn, whereas decreasing passenger weight and mission range decreases fuel burn.

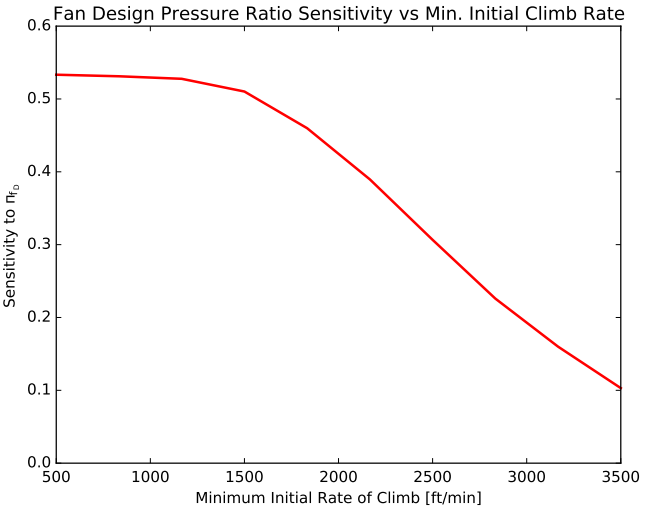

Fig. 15 Sensitivity to fan design pressure ratio vs minimum initial climb rate.

Downloaded by MASSACHUSETTS INST OF TECHNOLOGY on November 24, 2017 | http://arc.aiaa.org | DOI: 10.2514/1.C034463

It is also interesting to analyze how sensitivities change as mission parameters change. Figure 15 is a plot of the sensitivity to the fan design pressure ratio versus minimum initial climb rate. Initially, it is quite beneficial to decrease the fan design pressure ratio, as indicated by the sensitivity of approximately 0.53. However, as the minimum climb rate increases and the maximum thrust requirement on the engine increases, it becomes less beneficial to decrease the fan design pressure ratio. This is indicated by the decrease in sensitivity to approximately 0.1 for a minimum climb rate of 3500 ft/ min.

VII. Conclusions

This paper has presented a full 1-D core and fan flowpath physics-based, signomial programming compatible, turbofan model that was successfully validated against TASOPT and two NPSS models developed by the Georgia Institute of Technology. The model is meant to be combined with other aircraft subsystem models to perform full system optimization. Using GPkit's performance modeling framework, the turbofan model was formulated as a unified multipoint optimization problem with no on/ off-design point distinction or order of operations. The model can be easily be integrated into a full aircraft optimization model. This was demonstrated by integrating the turbofan model into a simple commercial aircraft sizing model and performing a series of parametric studies, including a 2480-variable multimission optimization problem that solves in 3.71 s.

Appendix A: Diffuser, Fan, and Compressor Model

Isentropic relations and a freestream Mach number, static pressure, and airspeed are used to constrain inlet stagnation quantities. When the engine model is used as part of a full aircraft optimization model, the ambient atmospheric properties and M_0 are linked to atmosphere and flight profile models. These values are set by the user if the engine is run in isolation. Diffuser boundary layer growth is neglected, and a specified diffuser pressure ratio accounts for diffuser stagnation pressure drop. The constraints governing this are presented next. Z_0 replaces the non-GP-compatible expression $1 + ((\gamma - 1)/2)(M_0)^2$ in the stagnation relations:

$$\begin{aligned} a_0 &= \sqrt{\gamma R T_0} \\ u_0 &= M_0 a_0 \\ P_{t_0} &= P_0 Z_0^{3.5} \\ T_{t_0} &= T_0 Z_0 \\ h_{t_0} &= C_{p_{\text{air}}} T_{t_0} \\ P_{t_2} &= \pi_d P_{t_0} \\ T_{t_2} &= T_{t_0} \\ h_{t_2} &= h_{t_0} \end{aligned} \tag{A1}$$

State changes across the fan, LPC, and HPC are computed using isentropic relations and user-specified polytropic efficiencies:

$$\begin{aligned} P_{t_{i+1}} &= \pi_i P_{t_i} \\ T_{t_{i+1}} &= T_{t_i} \pi_i^{[(\gamma_i - 1)/\eta_i \gamma_i]} \\ h_{t_{i+1}} &= C_{p_i} T_{t_i} \end{aligned} \tag{A2}$$

Appendix B: Turbine Model

The low-pressure turbine (LPT) must supply enough power to drive the fan and LPC. The high-pressure turbine (HPT) must supply enough power to drive the HPC. This is ensured by enforcing the following two shaft power balance constraints, both of which are signomial equalities. $\bar{f}_o$ is equal to 1 minus the percent of mass flow bled to provide pressurization and deice ($1\text{-}\dot{m}_{\text{offtake}}/\dot{m}_{\text{core}}$). Shaft power offtakes for customer power are smeared into the shaft power transmission efficiencies $\eta_{\text{HP/LP}}$:

$$\bar{f}_o \eta_{\text{HP}} (1 + f_f)(h_{t_{4.1}} - h_{t_{4.5}}) = (h_{t_3} - h_{t_{2.5}}) \tag{B1}$$

$$\bar{f}_o \eta_{\text{LP}} (1 + f_f)(h_{t_{4.9}} - h_{t_{4.5}}) = \alpha_{+1}(h_{t_{2.1}} - h_{t_2}) + (h_{t_{1.8}} - h_{t_{2.5}}) \tag{B2}$$

The isentropic relations and user-specified component polytropic efficiencies determine fluid states at stations 4.5 and 4.9:

$$P_{t_{i+1}} = \pi_i P_{t_i} \tag{B3}$$

$$\pi_i = \left(\frac{T_{t_{i+1}}}{T_{t_i}} \right)^{\eta_i \gamma_i / (\gamma_i - 1)} \tag{B4}$$

$$h_{t_{i+1}} = C_{p_i} T_{t_i} \tag{B5}$$

Appendix C: Flight Profile and Aircraft Sizing Model

The aircraft sizing model and flight profile model sizes a commercial aircraft for minimum fuel burn during a flight of user-specified range. The model is discretized into a user-selected number of climb and cruise flight segments. Descent is neglected. To avoid introducing a signomial, the downrange distance traveled during climb does not contribute to total mission range. Aircraft model nomenclature is presented in Table C1.

C.I. Weight Breakdown

The payload is taken to be only passengers and their baggage. Per-passenger total weight (person and baggage) is assumed to be 210 lb, and the number of passengers, N_{pax}, is specified by the user. The empty fuselage and tail weight is approximated as 75% of the payload weight. The 75% fraction is estimated from TASOPT 737 output. Wing weight is computed using a simplified Raymer wing weight equation normalized by TASOPT 737 wing weight, area, and aspect ratio values [20] in Eq. (C3). Total fuel burn is the sum of segment fuel burn:

$$W_{\text{payload}} = W_{\text{pax}} N_{\text{pax}} \tag{C1}$$

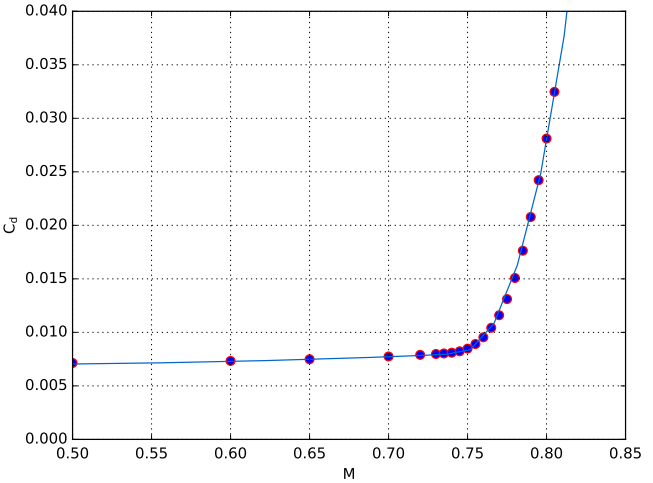

Fig. C1 Xfoil NC130 airfoil drag data (dots) and a posynomial approximation of the data (solid line) for a Reynolds number of 20 million.

Downloaded by MASSACHUSETTS INST OF TECHNOLOGY on November 24, 2017 | http://arc.aiaa.org | DOI: 10.2514/1.C034463

Table C1 Basic aircraft model nomenclature

Parameter	Definition
A_{fuse}	Projected fuselage area
A_{pax}	Required fuselage area per passenger
$\mathcal{AR}$	Wing aspect ratio
b	Wing span
$b_{\max}$	Maximum allowed wing span
$C_{d_{\text{fuse}}}$	Fuselage drag coefficient
C_{d_w}	Wing drag coefficient
D	Total aircraft drag
ΔH	Altitude change
K	Induced drag correction factor
N_{eng}	Aircraft's number of engines
N_{pax}	Aircraft's number of passengers
θ	Climb angle
h	Altitude
L	Temperature lapse rate in the troposphere
P_{excess}	Excess power
Range	Downrange distance covered
RC	Rate of climb
S	Wing planform area
t	Flight segment duration
V_{stall}	Aircraft stall speed
W_{avg}	Average flight segment aircraft weight
W_{end}	Aircraft flight segment end weight
W_{fuel}	Flight segment fuel weight burned
$W_{\text{fuel}_{\text{total}}}$	Total fuel weight
W_{fuse}	Fuselage weight
W_{pax}	Passenger weight
W_{payload}	Payload weight
W_{S}	Wing loading
$W_{\text{S}_{\max}}$	Maximum allowed wing loading
W_{start}	Aircraft flight segment start weight
W_{TO}	Takeoff weight
W_{wing}	Wing weight
z_{bre}	Breguet parameter
$(\cdot)_{\ldots i}$	Flight segment i quantity

$$W_{\text{fuse}} = 0.75 W_{\text{payload}} \tag{C2}$$

$$\left(\frac{S}{124.58\text{m}^2}\right)^{0.65}\left(\frac{AR}{10.1}\right)^{0.5} = \frac{W_{\text{wing}}}{105384.1524\text{N}} \tag{C3}$$

$$W_{\text{fuel}_i} = N_{\text{eng}}\text{TSFC}_i t_i F_i \tag{C4}$$

$$W_{\text{fuel}_{\text{total}}} \geq \sum_{n=1}^{N} W_{\text{fuel}_i} \tag{C5}$$

The aircraft's takeoff weight is the sum of all previously computed weights. Engine weight, W_{eng}, is set by the linked turbofan model. N_{eng} is the user-input number of engines:

$$W_{\text{TO}} \geq W_{\text{fuse}} + W_{\text{payload}} + W_{\text{fuel}_{\text{total}}} + N_{\text{eng}} W_{\text{eng}} + W_{\text{wing}} \tag{C6}$$

Equations (C7–C9) set each flight segment's start and end weight:

$$W_{\text{start}_i} = W_{\text{end}_{i-1}} \tag{C7}$$

$$W_{\text{start}_0} = W_{\text{TO}} \tag{C8}$$

$$W_{\text{end}_i} \geq W_{\text{empty}} + W_{\text{payload}} + N_{\text{eng}} W_{\text{eng}} + W_{\text{wing}} \tag{C9}$$

In later constraints, W_{avg_i}, the geometric mean of a segment's start and end weight, is used instead of either the segment start or end weight. This increases accuracy and is more stable than using segment start or end weight:

$$W_{\text{avg}_i} = \sqrt{W_{\text{start}_i} W_{\text{end}_i}} \tag{C10}$$

C.II. Aircraft Sizing

To capture landing/takeoff constraints, wing loading is constrained to be less than a user-specified maximum value. Aspect ratio, $\mathcal{AR}$, is set by the wing span and wing area and constrained to be less than a user-input maximum value. There is no wing structural model. Without the user-input maximum value, the aspect ratio would grow unrealistically large:

$$W_{S_i} = \frac{(1/2)C_{L_i} S \rho_i (V_i)^2}{S} \tag{C11}$$

$$W_{S_i} \leq W_{S_{\max}} \tag{C12}$$

$$\mathcal{AR} = \frac{b^2}{S} \tag{C13}$$

$$\mathcal{AR} \leq \mathcal{AR}_{\max} \tag{C14}$$

To capture trends in fuselage drag, the fuselage is approximated as a flat plate. The plate's area is a function of number of passengers; the area per passenger, N_{pax}, is estimated as 1 m^2 per passenger. The estimate is based off the per passenger projected fuselage areas of late model 737s and 777s:

$$A_{\text{fuse}} = A_{\text{pax}} N_{\text{pax}} \tag{C15}$$

The drag coefficient of a turbulent flat plate parallel to the freestream is 0.005. Fuselage drag can then be approximated as $C_{d_{\text{fuse}}} = (1/2)\rho V^2 A_{\text{fuse}} C_{d_{\text{fuse}}}$, where $C_{d_{\text{fuse}}} = 0.005$.

C.III. General Aircraft Performance

A number of constraints apply to both the climb and cruise portions of the flight. The speed of sound, velocity, and Mach number are computed for each flight segment. Velocity is also constrained to be greater than a user-input stall speed. Segment lift, $(1/2)\rho_i C_{L_i}(V_i)^2$, is equated to the segment's average weight:

$$a_i = \sqrt{\gamma R T_i} \tag{C16}$$

$$V \geq V_{\text{stall}} \tag{C17}$$

$$V_i = a_i M_i \tag{C18}$$

$$W_{\text{avg}_i} = \frac{1}{2}\rho_i C_{L_i}(V_i)^2 \tag{C19}$$

Drag is computed with Eq. (C21). The parabolic drag model, with the induced drag parameter K, is used to model induced drag. GPfit [14,15] was used to develop a GP-compatible fit to Xfoil [21] drag

data for an NC130 airfoil [4] at a Reynolds number of 20 million. The fit is plotted in Fig. C1. Equation (C20), which sets C_{d_w}, was derived from the data fit:

$$C_{d_w} \geq (1.025e10)C_L^{15.58}M^{156.86} + (2.856e-13)C_L^{1.28}M^{6.25} + (2.091e-14)C_L^{0.88}M^{0.03} + (1.944e6)C_L^{5.65}M^{146.52} \quad \text{(C20)}$$

$$D_i \geq \left(\frac{1}{2}\rho_i(V_i)^2\right)(C_{d_w} + K(C_L)^2 + C_{D_{\text{fuse}}}A_{\text{fuse}}) \quad \text{(C21)}$$

$$K = (\pi e \mathcal{AR})^{-1} \quad \text{(C22)}$$

C.IV. Climb

The climb rate is set with an excess power formulation [22] and constrained to be greater than 500 ft/min. Equation (C26) uses a small-angle approximation to set the climb angle θ:

$$P_{\text{excess}} + V_i D_i \leq V_i N_{\text{eng}} F_i \quad \text{(C23)}$$

$$\text{RC}_i = \frac{P_{\text{excess}}}{W_{\text{avg}_i}} \quad \text{(C24)}$$

$$\text{RC}_i \geq 500 \text{ ft/min} \quad \text{(C25)}$$

$$\theta_i V_i = \text{RC}_i \quad \text{(C26)}$$

Altitude change during each climb segment is a function of climb rate and total segment time. Equation (C28) uses a small-angle approximation to compute the downrange distance covered during a climb segment. This distance is not credited toward the aircraft's mission range:

$$\Delta H_i = t_i \text{RC}_i \quad \text{(C27)}$$

$$t_i V_i = \text{Range}_i \quad \text{(C28)}$$

During climb, there is a downward pressure on each segment's end altitude (climbing extra burns more fuel). This allows each climb segment's end altitude to be computed with Eq. (C29):

$$h_i \geq h_{i-1} + \Delta H_i \quad \text{(C29)}$$

C.V. Cruise

Steady level flight conditions are assumed during cruise. Flight segment duration is constrained via Eq. (C31). This is the same equation as Eq. (C28), except it does not use a small-angle approximation:

$$D_i = N_{\text{eng}} F_i \quad \text{(C30)}$$

$$t_i V_i = \text{Range}_i \quad \text{(C31)}$$

The Breguet range equation [Eq. (C32)] is used to model cruise fuel burn. However, the natural logarithm in Eq. (C32) is not GP-compatible and must be reformulated using the procedure outlined by Hoburg and Abbeel [2]. Equations (C33, C34) constitute the reformulated Breguet range equation. W_i in Eq. (C32) has been replaced with W_{avg_i} to increase accuracy:

$$\ln\left(\frac{W_{\text{start}_i}}{W_{\text{end}_i}}\right) = \frac{D_i(\text{TSFC}_i t_i)}{W} \quad \text{(C32)}$$

$$z_{\text{bre}} + \frac{{z_{\text{bre}}}^2}{2} + \frac{{z_{\text{bre}}}^3}{6} \leq \frac{W_{\text{fuel}}}{W_{\text{end}}} \quad \text{(C33)}$$

$$z_{\text{bre}} \geq \frac{D_i(\text{TSFC}_i)}{W_{\text{avg}_i}} t_i \quad \text{(C34)}$$

C.VI. Atmosphere Model

Equation (C35), a signomial equality, is used to compute each flight segment's temperature (h is linked to segment end altitude). Atmospheric pressure is computed with the hydrostatic equation, and density is computed with the ideal gas law. L_{atm} is the standard temperature lapse rate (0.0065 K/m), R is the universal gas constant, M is the gasses molar mass, T_{SL} is sea-level temperature, and P_{SL} is the sea-level pressure:

$$T_{\text{SL}} = T + L_{\text{atm}} h \quad \text{(C35)}$$

$$\left(\frac{P}{P_{\text{SL}}}\right)^{LR/g} = \frac{T}{T_{\text{SL}}} \quad \text{(C36)}$$

$$\rho = \frac{P}{(R/M)T} \quad \text{(C37)}$$

Appendix D: Signomial Equality Constraint Intuition

Signomial equality constraints are required when one variable in a signomial is being pressured in multiple different directions or a posynomial inequality will not remain tight. Consider the constraints used in a simple atmosphere model integrated into an aircraft mission profile. L is the standard the temperature lapse rate of 0.0065 K/m, and T_{SL} and P_{SL} are the sea-level temperature and pressure, respectively:

$$\rho = \frac{P}{RT}, \qquad \left(\frac{P}{P_{\text{SL}}}\right)^{LR/g} = \frac{T}{T_{\text{SL}}}, \qquad T_{\text{SL}} = T + Lh \quad \text{(D1)}$$

It is not clear a priori how to relax the posynomial equality $T_{\text{SL}} = T + Lh$ to an inequality. During the climb phase of the flight, there will be an upward pressure on density (higher density allows a higher climb rate), creating a downward pressure on T. During the cruise portion of the flight, there will be a downward pressure on density (lower density produces less drag on the aircraft), creating an upward pressure on T. Situations like this require signomial equality constraints.

Within the engine model, the variables α_{+1} and f_{f+1} are introduced to limit the total number of signomial equalities in the model. Both must be defined via signomial equalities. There is an upward pressure on α (engines with a larger bypass ratio tend to be more efficient) and α_{+1} due to Eq. (62), so the GP-compatible posynomial inequality $\alpha_{+1} \geq \alpha + 1$ would not remain tight. Similarly, an upward pressure on f_{f+1} can be generated within the nominal design point estimation constraints in Sec. IV.B, so the constraint $f_{f+1} \geq f + 1$ would not remain tight:

$$\alpha_{+1} = \alpha + 1 \quad \text{(D2)}$$

$$f_{f+1} = f_f + 1 \quad \text{(D3)}$$

Acknowledgment

This work was partially funded by Aurora Flight Sciences.

Downloaded by MASSACHUSETTS INST OF TECHNOLOGY on November 24, 2017 | http://arc.aiaa.org | DOI: 10.2514/1.C034463

References

[1] Martins, J. R., and Lambe, A. B., "Multidisciplinary Design Optimization: A Survey of Architectures," *AIAA Journal*, Vol. 51, No. 9, 2013, pp. 2049–2075.

[2] Hoburg, W., and Abbeel, P., "Geometric Programming for Aircraft Design Optimization," *AIAA Journal*, Vol. 52, No. 11, 2014, pp. 2414–2426.

[3] Kirschen, P. G., Burnell, E. E., and Hoburg, W. W., "Signomial Programming Models for Aircraft Design," *54th AIAA Aerospace Sciences Meeting*, AIAA Paper 2016-2003, 2016.

[4] Drela, M., "N3 Aircraft Concept Designs and Trade Studies – Appendix," NASA CR-2010-216794, Vol. 2, 2010.

[5] "Numerical Propulsion System Simulation," Southwest Research Inst, San Antonio, TX, http://www.swri.org/npss/purchase.asp [retrieved Aug. 2016].

[6] Burnell, E., and Hoburg, W., "GPkit Software for Geometric Programming," Software Package, Ver. 0.4.0, 2015, https://github.com/hoburg/gpkit [retrieved June 2016].

[7] "The MOSEK C Optimizer API Manual," Ver. 7.1, Rev. 41, Mosek, 2015.

[8] Duffin, R., Peterson, E., and Zener, C., *Geometric Programming: Theory and Application*, Wiley, New York, 1967.

[9] Boyd, S., and Vandenberghe, L., *Convex Optimization*, 7th ed., Cambridge Univ. Press, New York, 2009, pp. 8, 160–167.

[10] Boyd, S., Kim, S.-J., Vanderberghe, L., and Hassibi, A., "A Tutorial on Geometric Programming," *Optimization and Engineering*, Vol. 8, 2007, pp. 67–127.

[11] Lipp, T., and Boyd, S., "Variations and Extension of the Convex Concave Procedure," *Optimization and Engineering*, Vol. 17, 2015, pp. 263–287.

[12] Opgenoord, M. M. J., Cohen, B. S., and Hoburg, W. W., "Comparison of Algorithms for Including Equality Constraints in Signomial Programming," Aerospace Computational Design Lab., Massachusetts Inst. of Technology, TR-17-1, Cambridge, MA, 2017.

[13] "Energy Efficient Engine Flight Propulsion System Aircraft/Engine Integration Evaluation," NASA CR-159584, 1980.

[14] Hoburg, W., Kirschen, P., and Abbeel, P., "Data Fitting with Geometric-Programming-Compatible Softmax Functions," *Optimization and Engineering*, Vol. 17, 2016, pp. 897–918.

[15] Kirschen, P., and Hoburg, W., "GPfit," Software Package, Ver. 0.1, 2015, https://github.com/convexopt/gpfit [retrieved June 2016].

[16] Marvis, D., "Environmental Design Space (EDS) Overview," *Presentation to the Transportation Research Board, Papers and Briefings on the Development Program for the Aviation Environmental Tool Suite, Workshop No. 4*, TR, 2010, http://onlinepubs.trb.org/onlinepubs/archive/Conferences/AEDT-APMT/05_DM_Overview-EDS_2006-11-28_FINAL.pdf [retrieved Aug. 2016].

[17] CFM International, https://www.cfmaeroengines.com/engines/cfm56 [retrieved Aug. 2016].

[18] "Jet Fuel Product Properties," ExxonMobil, https://www.exxonmobil.com/English-FI/Commercial-Fuel/pds/GLXXJetFuel-Series [retrieved June 2016].

[19] Yutko, B., "The Impact of Aircraft Design Reference Mission on Fuel Efficiency in the Air Transportation System," Ph.D. Thesis, Massachusetts Inst. of Technology, Cambridge, MA, 2013.

[20] Raymer, D. P., *Aircraft Design: A Conceptual Approach*, 2nd ed., AIAA, Washington D.C., 1992, p. 403.

[21] Drela, M., "XFOIL: An Analysis and Design System for Low Reynolds Number Airfoils," *Low Reynolds Number Aerodynamics*, edited by T. J. Mueller, Vol. 54, Lecture Notes in Engineering, Springer, Berlin, 1989, pp. 1–12.

[22] Anderson, J. D., *Aircraft Performance and Design*, WCB McGraw–Hill, Boston, MA, 1999, pp. 265–270.

Downloaded by MASSACHUSETTS INST OF TECHNOLOGY on November 24, 2017 | http://arc.aiaa.org | DOI: 10.2514/1.C034463